Ultra-large-scale syntheses of monodisperse nanocrystals

JONGNAM PARK[1], KWANGJIN AN[1], YOSUN HWANG[2], JE-GEUN PARK[2], HAN-JIN NOH[3], JAE-YOUNG KIM[3], JAE-HOON PARK[3], NONG-MOON HWANG[4] AND TAEGHWAN HYEON[1]*

[1]National Creative Research Center for Oxide Nanocrystalline Materials and School of Chemical Engineering, Seoul National University, Seoul 151-744, Korea
[2]Department of Physics and Institute of Basic Science, Sungkyunkwan University, Suwon 440-746, Korea
[3]Department of Physics and Pohang Light Source, Pohang University of Science and Technology, Pohang 790-784, Korea
[4]School of Materials Science & Engineering and Nano-Systems Institute (NSI-NCRC), Seoul National University, Seoul 151-744, Korea
*e-mail: thyeon@plaza.snu.ac.kr

Published online: 28 November 2004; doi:10.1038/nmat1251

The development of nanocrystals has been intensively pursued, not only for their fundamental scientific interest, but also for many technological applications[1–3]. The synthesis of monodisperse nanocrystals (size variation <5%) is of key importance, because the properties of these nanocrystals depend strongly on their dimensions. For example, the colour sharpness of semiconductor nanocrystal-based optical devices is strongly dependent on the uniformity of the nanocrystals[3–6], and monodisperse magnetic nanocrystals are critical for the next-generation multi-terabit magnetic storage media[7–9]. For these monodisperse nanocrystals to be used, an economical mass-production method needs to be developed. Unfortunately, however, in most syntheses reported so far, only sub-gram quantities of monodisperse nanocrystals were produced. Uniform-sized nanocrystals of CdSe (refs 10,11) and Au (refs 12,13) have been produced using colloidal chemical synthetic procedures. In addition, monodisperse magnetic nanocrystals such as Fe (refs 14,15), Co (refs 16–18), γ-Fe_2O_3 (refs 19,20), and Fe_3O_4 (refs 21,22) have been synthesized by using various synthetic methods[23]. Here, we report on the ultra-large-scale synthesis of monodisperse nanocrystals using inexpensive and non-toxic metal salts as reactants. We were able to synthesize as much as 40 g of monodisperse nanocrystals in a single reaction, without a size-sorting process. Moreover, the particle size could be controlled simply by varying the experimental conditions. The current synthetic procedure is very general and nanocrystals of many transition metal oxides were successfully synthesized using a very similar procedure.

The process conditions required for the synthesis of monodisperse particles of micrometre size[24] are relatively well established, and a similar principle could be applied to the synthesis of uniform-sized nanocrystals. The inhibition of additional nucleation during growth, in other words, the complete separation of nucleation and growth, is critical for the successful synthesis of monodisperse nanocrystals. Our research group developed new procedures for the synthesis of monodisperse nanocrystals of metals[19,23,25], metal oxides[19,26,27], and metal sulphides[28] without a laborious size-sorting process. In particular, during the direct synthesis of monodisperse iron and iron oxide nanocrystals[19,23], we were able to ascertain that the iron–oleate complex, which is generated *in situ* from the reaction of iron pentacarbonyl and oleic acid, is decomposed and acts effectively as a growth source in synthesizing monodisperse nanocrystals with increased particle size. From these results, we reasoned that a metal–surfactant complex would make an effective growth source for the synthesis of monodisperse nanocrystals. The overall synthetic procedure is depicted in Fig. 1 and the detailed experimental procedures are described in the Methods section. Instead of using toxic and expensive organometallic compounds such as iron pentacarbonyl, we prepared the metal–oleate complex by reacting inexpensive and environmentally friendly compounds, namely metal chlorides and sodium oleate. The Fourier transform infrared spectrum of the iron–oleate complex, which was prepared by reacting iron chloride ($FeCl_3{\cdot}6H_2O$) and sodium oleate, shows a C=O stretching peak at 1,700 cm^{-1}, which is a characteristic peak for a metal–oleate complex (see Supplementary Information, Fig. S1). The iron–oleate complex in 1-octadecene was slowly heated

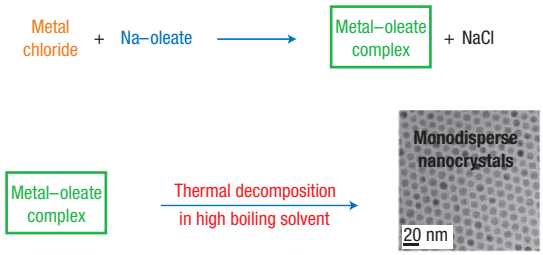

Figure 1 The overall scheme for the ultra-large-scale synthesis of monodisperse nanocrystals. Metal–oleate precursors were prepared from the reaction of metal chlorides and sodium oleate. The thermal decomposition of the metal–oleate precursors in high boiling solvent produced monodisperse nanocrystals.

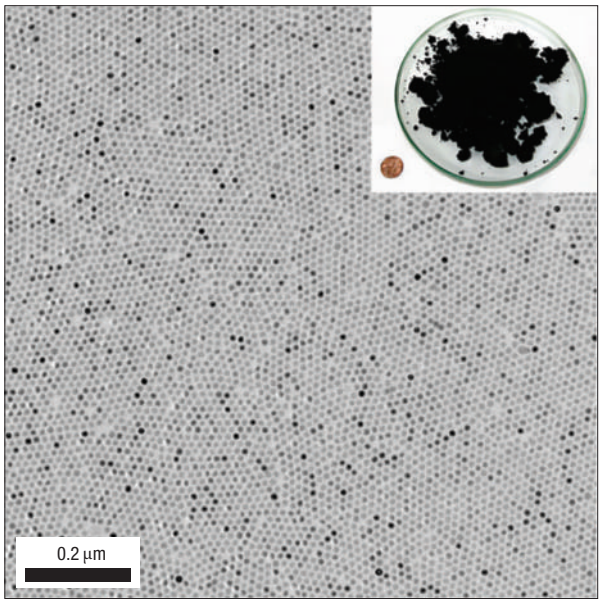

Figure 2 12-nm magnetite nanocrystals. The TEM image clearly demonstrates that the nanocrystals are highly uniform in particle-size distribution. Inset is a photograph showing a Petri dish containing 40 g of the monodisperse magnetite nanocrystals, and a US one-cent coin for comparison.

to 320 °C, and was aged at that temperature for 30 min, generating iron oxide nanocrystals. The amount of the separated nanocrystals produced was as large as 40 g with a yield of >95%. The nanocrystals could easily be re-dispersed in various organic solvents including hexane and toluene.

To understand the mechanism of monodisperse nanoparticle formation, we obtained transmission electron microscope (TEM; JEOL EM-2010) images and conducted *in situ* infrared spectroscopy on the reaction mixture after heating at various temperatures and for various times. We also investigated the thermal decomposition behaviour of the solid-state iron–oleate precursor using thermogravimetric analysis (TGA), differential scanning calorimetry (DSC), and temperature-programmed infrared spectroscopy (see Supplementary Information). The TGA/DSC patterns and infrared spectra revealed that one oleate ligand dissociates from the precursor at 200–240 °C and the remaining two oleate ligands dissociate at ~300 °C by a CO_2 elimination pathway. The TEM image of the sample taken at 310 °C without aging showed that nanoparticles were not produced, whereas the TEM image taken at 320 °C revealed the formation of relatively uniform nanoparticles with sizes ranging from 8 nm to 11 nm. All the TEM images taken after aging at 320 °C for 10, 20 and 30 min showed monodisperse 12 nm nanoparticles. Aging at 260 °C for one day produced polydisperse and poorly crystalline 9 nm nanoparticles, and aging at the same temperature for three days generated monodisperse 12 nm nanocrystals. When aged at 240 °C for one day, no nanoparticles were formed, and aging at 240 °C for three days produced highly polydisperse ~14 nm nanoparticles. When aged at 200 °C for three days, no nanoparticles were formed.

From these TEM, DSC/TGA and infrared data, we could propose the following mechanism for the nanocrystal formation. Nucleation occurs at 200–240 °C triggered by the dissociation of one oleate ligand from the $Fe(oleate)_3$ precursor by CO_2 elimination. The major growth occurs at ~300 °C initiated by the dissociation of the remaining two oleate ligands from the iron–oleate species, although

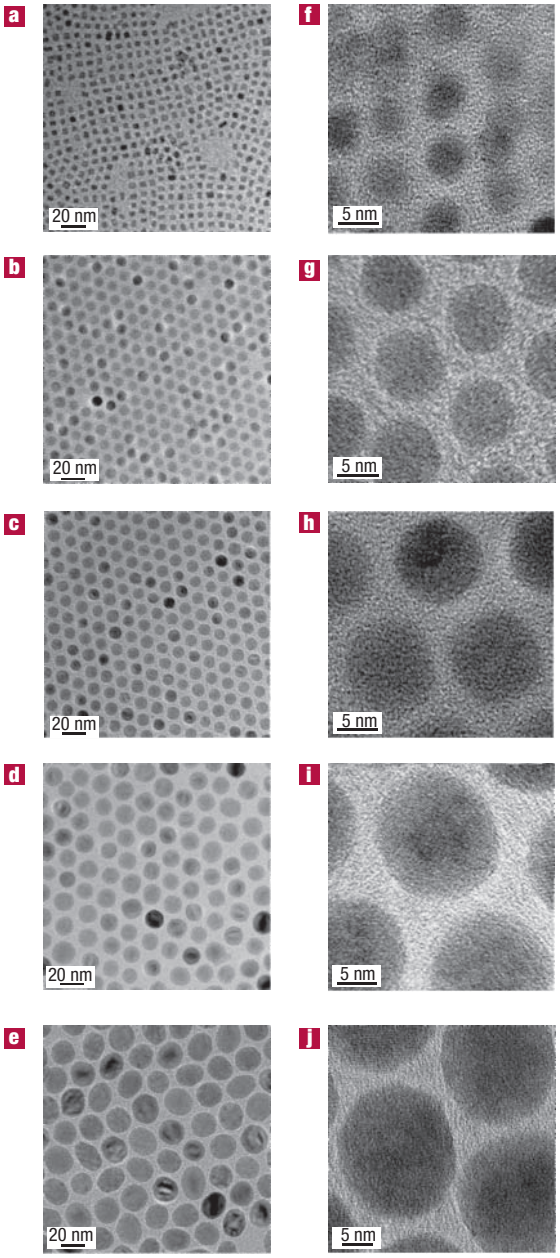

Figure 3 TEM images (a–e) and HRTEM images (f–j) of monodisperse iron oxide nanocrystals. (**a**, **f**) 5 nm; (**b**, **g**) 9 nm; (**c**, **h**) 12 nm; (**d**, **i**) 16 nm; and (**e**, **j**) 22 nm nanocrystals. TEM images showed the highly monodisperse particle size distributions and HRTEM images revealed the highly crystalline nature of the nanocrystals.

slow growth seems to occur at <250 °C. Consequently, we were able to synthesize monodisperse nanocrystals from the separation of nucleation and growth processes, which tend to take place at different temperatures. Because the growth process is time-dependent, when the precursor was aged at a low temperature of 240 °C (close to the nucleation temperature) for three days, we obtained polydisperse nanocrystals. These results imply that the current successful synthesis of monodisperse nanocrystals can be attributed to the effective separation of nucleation and growth processes, which result from the different temperature dependence of nucleation and growth kinetics.

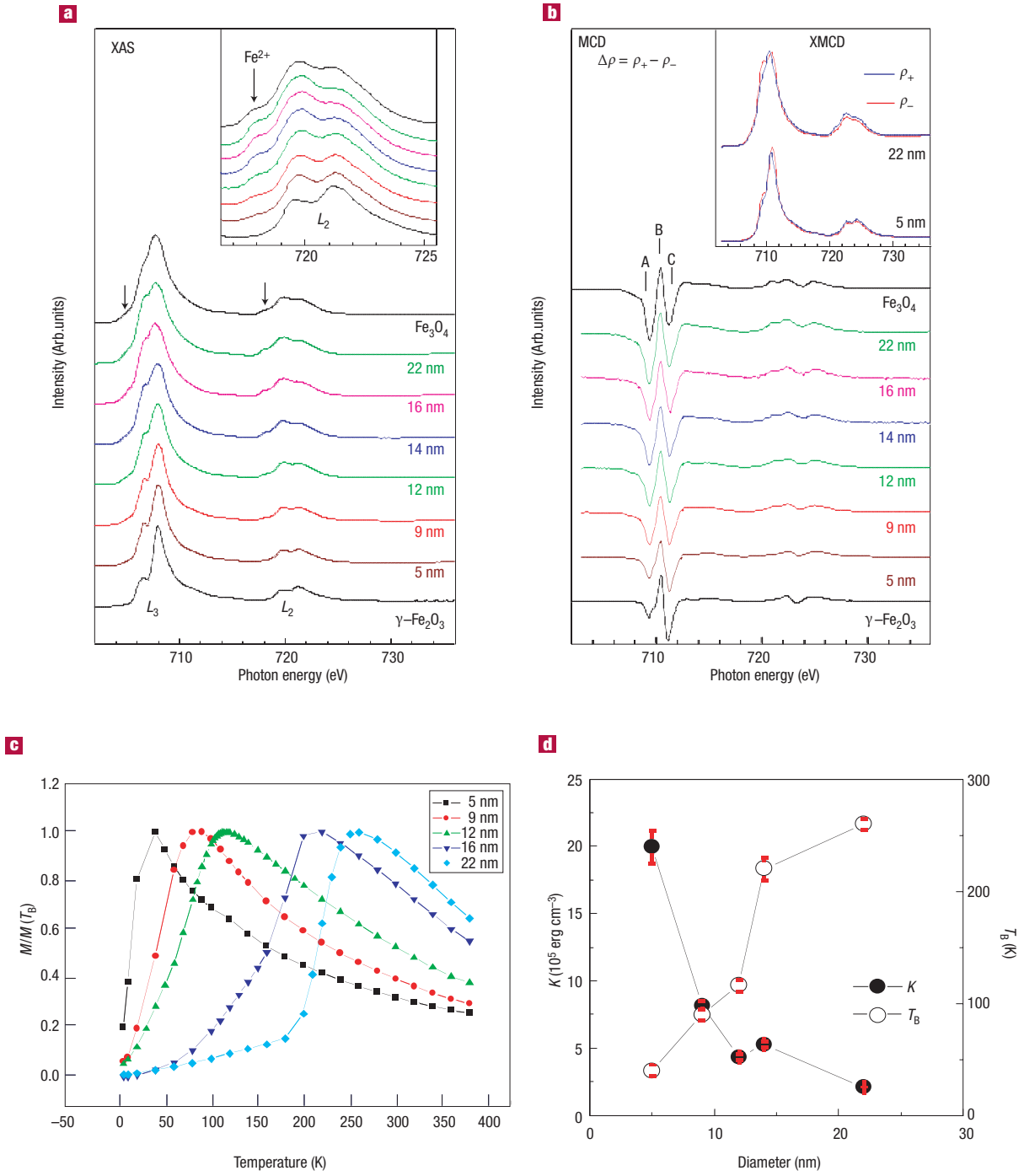

Figure 4 Characterization of monodisperse iron oxide nanocrystals. **a**, Fe $L_{2,3}$-edge XAS and **b**, XMCD spectra of iron oxide nanocrystals in comparison with those of reference bulk materials, γ-Fe_2O_3 and Fe_3O_4. The magnified L_2 region XAS spectra and the XMCD spectra of the 5 nm and 22 nm nanocrystals are shown in the insets of **a** and **b**, respectively. In the inset of **b**, ρ_+ and ρ_- represent the absorption coefficients for the photon helicity vector parallel and antiparallel to the magnetization direction of the nanocrystals, respectively. **c**, Temperature dependence of magnetization measured after zero-field cooling (ZFC) using 100 Oe. For the sake of presentation, we have normalized the magnetization data with respect to the value at the maximum of ZFC magnetization, $M(T_B)$, for individual samples. **d**, Size dependence of T_B, obtained from $M(T)$ shown in **c**.

The nanocrystals were characterized using TEM, X-ray diffraction (XRD; Rigaku D/Max-3C)), X-ray absorption spectroscopy (XAS), and X-ray magnetic circular dichroism spectroscopy (XMCD). The TEM image of the iron oxide nanocrystals synthesized at the 40-g scale in a single reaction using 200 g of solvent, shown in Fig. 2, exhibited an extensive 2D assembly of uniform 12-nm nanocrystals, demonstrating their monodisperse particle size distribution (size variation = 2.3%, see Supplementary Information). A photograph of a Petri dish containing 40 g of the nanocrystals is shown in the inset of Fig. 2. The particle size of the iron oxide nanocrystals could

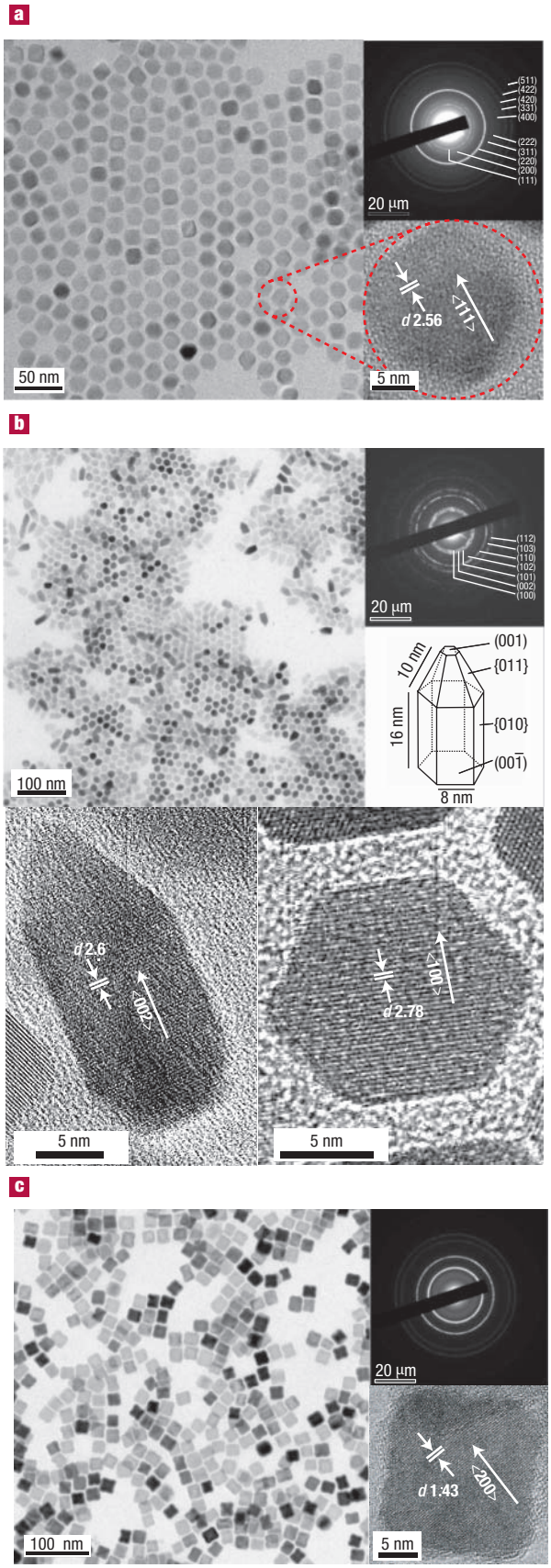

Figure 5 TEM images, HRTEM images and electron diffraction patterns of monodisperse nanocrystals. **a**, MnO, **b**, CoO and **c**, Fe. TEM images show the highly uniform characteristics of the nanocrystals in terms of both particle size and particle shape. HRTEM images and electron diffraction patterns revealed the highly crystalline nature of the nanocrystals.

be controlled by using various solvents with different boiling points. As shown in Fig. 3, 5 nm (a, TEM; and f, high-resolution TEM), 9 nm (b and g), 12 nm (c and h), 16 nm (d and i), and 22 nm (e and j) iron oxide nanocrystals were synthesized using 1-hexadecene (b.p. 274 °C), octyl ether (b.p. 287 °C), 1-octadecene (b.p. 317 °C), 1-eicosene (b.p. 330 °C) and trioctylamine (b.p. 365 °C), respectively. All the nanocrystals are highly monodisperse in particle-size distribution (size variation <4.1%, see Supplementary Information). As the boiling point of the solvent increased, the diameter of the iron oxide nanocrystals increased. This result can be explained by the higher reactivity of the iron–oleate complex in the solvent with a higher boiling point. High-resolution TEM (HRTEM) images of these iron oxide nanocrystals showed distinct lattice fringe patterns, indicating the highly crystalline nature of the nanocrystals (Fig. 3f–j). The size of the iron oxide nanocrystals can be further fine-tuned by varying the concentration of oleic acid. For example, 11 nm, 12 nm and 14 nm iron oxide nanocrystals were synthesized using solutions with oleic acid concentrations of 1.5 mM, 3 mM and 4.5 mM, respectively (see Supplementary Information).

The XRD pattern of the 12-nm iron oxide nanocrystals revealed a cubic spinel structure of magnetite (see Supplementary Information). For the quantitative identification of the compositions of the iron oxide nanocrystals, XAS and XMCD measurements at the Fe $L_{2,3}$-edges were carried out at the EPU6 beamline at the Pohang Light Source. Figure 4a,b shows XAS spectra and XMCD results of the iron oxide nanocrystals with diameters of 5 nm, 9 nm, 12 nm, 16 nm and 22 nm, in comparison with those of two reference materials, bulk γ-Fe_2O_3 (maghemite) and bulk Fe_3O_4 (magnetite), which have nearly the same spinel crystal structure with only ~1% difference in the cubic lattice constant. Both the XAS and MCD spectra of the 5 nm nanoparticles are very similar to those of γ-Fe_2O_3, which contains only Fe^{3+}. From the XAS and XMCD results, we made a quantitative estimation of the compositions for the iron oxide nanocrystals in the form of $(\gamma\text{-}Fe_2O_3)_{1-x}(Fe_3O_4)_x$. The estimations are x = 0.20, 0.57, 0.68, 0.86 and 1.00 for the 5, 9, 12, 16 and 22 nm nanocrystals, respectively. Therefore, γ-Fe_2O_3 is the dominant phase of the small 5-nm iron oxide nanocrystals, whereas the proportion of the Fe_3O_4 component gradually increases on increasing the particle size.

The magnetic properties of these iron oxide nanocrystals were studied using a commercial superconducting quantum interference device magnetometer (Quantum Design, MPMS5XL). Figure 4c shows the temperature dependence of magnetization measured with an applied magnetic field of 100 Oe from 380 K to 5 K. All of our nanocrystals show superparamagnetic behaviour at high temperatures. However, on cooling, the zero-field-cooled magnetization begins to drop and deviate from the field-cooled magnetization at blocking temperature, T_B. T_B is at 40 K for the 5 nm sample, T_B increases continuously as the diameter of the nanocrystals increases: for example, to 260 K for the 22 nm nanocrystals (Fig. 4d). From the measured T_B, we calculated the magnetic anisotropy constant, K, using the equation: $K = 25k_BT_B/V$, where k_B is Boltzmann's constant and V is the volume of a single nanocrystal. As is typical of nanocrystals, the calculated magnetic anisotropy constant was found to increase with decreasing particle size (Fig. 4d).

The current synthetic procedure turned out to be widely applicable, and we successfully synthesized nanocrystals of many

transition metal oxides from the thermolysis of metal–oleate complexes. For example, when the Mn–oleate complex was refluxed in a solution containing octyl ether and oleic acid, uniform 12-nm f.c.c. MnO nanocrystals were synthesized (Fig. 5a). For the Co–oleate complex, short pencil-shaped CoO nanorods (Fig. 5b) were obtained. The CoO nanorods are uniform in diameter and form self-assembled superlattices (Fig. 5b). The XRD pattern of the CoO nanorods revealed an interesting Würtzite structure, similar to that of ZnO (see Supplementary Information). Furthermore, the (002) peak is narrower than the other peaks, demonstrating that the nanocrystals grow preferentially along the c axis. These results were confirmed by the subsequent HRTEM, which shows the (002) lattice spacing value of 2.6 Å (Fig. 5b). When the iron–oleate complex was heated at a higher temperature of 380 °C, novel cube-shaped 20-nm iron nanocrystals were produced. XRD and HRTEM analyses revealed that the surface of these Fe nanocubes is passivated by a thin FeO layer (Fig. 5c). Nanocrystals of manganese ferrite and cobalt ferrite were synthesized from the thermal decomposition of the reaction mixtures composed of 1:2 molar ratio of the corresponding metal–oleate complex and iron–oleate complex (see Supplementary Information).

The synthetic procedures developed in the present study offer several very important advantageous features over the conventional methods for the synthesis of monodisperse nanocrystals. First, this process allows monodisperse nanocrystals to be obtained on an ultra-large scale of 40 g in a single reaction and without a further size-sorting process. When the reactors are set up in parallel, multi-kilograms of monodisperse nanocrystals can be readily obtained. Second, the synthetic process is environmentally friendly and economical, because it uses non-toxic and inexpensive reagents such as metal chlorides[29]. Third, the synthetic method is a generalized process that can be used to synthesize different kinds of monodisperse nanocrystals.

METHODS

SYNTHESIS OF IRON–OLEATE COMPLEX

The metal–oleate complex was prepared by reacting metal chlorides and sodium oleate. In a typical synthesis of iron–oleate complex, 10.8 g of iron chloride ($FeCl_3{\cdot}6H_2O$, 40 mmol, Aldrich, 98%) and 36.5 g of sodium oleate (120 mmol, TCI, 95%) was dissolved in a mixture solvent composed of 80 ml ethanol, 60 ml distilled water and 140 ml hexane. The resulting solution was heated to 70 °C and kept at that temperature for four hours. When the reaction was completed, the upper organic layer containing the iron–oleate complex was washed three times with 30 ml distilled water in a separatory funnel. After washing, hexane was evaporated off, resulting in iron–oleate complex in a waxy solid form.

SYNTHESIS OF IRON OXIDE NANOCRYSTALS

The following is a typical synthetic procedure for monodisperse iron oxide (magnetite) nanocrystals with a particle size of 12 nm. 36 g (40 mmol) of the iron-oleate complex synthesized as described above and 5.7 g of oleic acid (20 mmol, Aldrich, 90%) were dissolved in 200 g of 1-octadecene (Aldrich, 90%) at room temperature. The reaction mixture was heated to 320 °C with a constant heating rate of 3.3 °C min^{-1}, and then kept at that temperature for 30 min. When the reaction temperature reached 320 °C, a severe reaction occurred and the initial transparent solution became turbid and brownish black. The resulting solution containing the nanocrystals was then cooled to room temperature, and 500 ml of ethanol was added to the solution to precipitate the nanocrystals. The nanocrystals were separated by centrifugation.

Received 11 June 2004; accepted 20 September 2004; published 28 November 2004.

References

1. Schmid, G. *Nanoparticles: From Theory to Application* (Wiley-VCH, Weinheim, 2004).
2. Klabunde, K. J. *Nanoscale Materials in Chemistry* (Wiley-Interscience, New York, 2001).
3. Alivisatos, A. P. Semiconductor clusters, nanocrystals, and quantum dots. *Science* **271,** 933–937 (1996).
4. Nirmal, M. & Brus, L. Luminescence photophysics in semiconductor nanocrystals. *Acc. Chem. Res.* **32,** 407–414 (1999).
5. Murray, C. B., Kagan, C. R. & Bawendi, M. G. Synthesis and characterization of monodisperse nanocrystals and close-packed nanocrystal assemblies. *Annu. Rev. Mater. Sci.* **30,** 545–610 (2000).
6. Rogach, A. L. *et al.* Organization of matter on different size scales: monodisperse nanocrystals and their superstructures. *Adv. Funct. Mater.* **12,** 653–664 (2002).
7. Sun, S., Murray, C. B. Weller, D., Folks, L. & Moser A. Monodisperse FePt nanoparticles and ferromagnetic FePt nanocrystal superlattices. *Science* **287,** 1989–1992 (2000).
8. Speliotis, D. E. Magnetic recording beyond the first 100 (invited). *J. Magn. Magn. Mater.* **193,** 29–35 (1999).
9. O'Handley, R. C. *Modern Magnetic Materials* (Wiley, New York, 1999).
10. Murray, C. B., Norris, D. J. & Bawendi, M. G. Synthesis and characterization of nearly monodisperse CdE (E = S, Se, Te) semiconductor nanocrystallites. *J. Am. Chem. Soc.* **115,** 8706–8715 (1993).
11. Peng, X., Wickham, J. & Alivisatos, A. P. Kinetics of II-VI and III-V colloidal semiconductor nanocrystal growth: "focusing" of size distributions. *J. Am. Chem. Soc.* **120,** 5343–5344 (1998).
12. Stoeva, S., Klabunde, K. J., Sorensen, C. M. & Dragieva, I. Gram-scale synthesis of monodisperse gold colloids by the solvated metal atom dispersion method and digestive ripening and their organization into two- and three-dimensional structures. *J. Am. Chem. Soc.* **124,** 2305–2311 (2002).
13. Jana, N. R. & Peng, X. Single-phase and gram-scale routes toward nearly monodisperse Au and other noble metal nanocrystals. *J. Am. Chem. Soc.* **125,** 14280–14281 (2003).
14. Park, S.-J. *et al.* Synthesis and magnetic studies of uniform iron nanorods and nanospheres. *J. Am. Chem. Soc.* **112,** 8581–8582 (2000).
15. Dumestre, F., Chaudret, B. Amiens, C., Renaud, P. & Fejes P. Superlattices of iron nanocubes synthesized from $Fe[N(SiMe_3)_2]_2$. *Science* **303,** 821–823 (2004).
16. Sun, S. & Murray, C. B. Synthesis of monodisperse cobalt nanocrystals and their assembly into magnetic superlattices (invited). *J. Appl. Phys.* **85,** 4325–4390 (1999).
17. Puntes, V. F., Krishnan, K. M. & Alivisatos, A. P. Colloidal nanocrystal shape and size control: the case of cobalt. *Science* **291,** 2115–2117 (2001).
18. Dumestre, F. *et al.* Shape control of thermodynamically stable cobalt nanorods through organometallic chemistry. *Angew. Chem. Int. Edn* **41,** 4286–4289 (2002).
19. Hyeon, T., Lee, S. S., Park, J., Chung, Y. & Na, H. B. Synthesis of highly crystalline and monodisperse maghemite nanocrystallites without a size-selection process. *J. Am. Chem. Soc.* **123,** 12798–12801 (2001).
20. Rockenberger, J., Scher, E. C. & Alivisatos, A. P. A new nonhydrolytic single-precursor approach to surfactant-capped nanocrystals of transition metal oxides. *J. Am. Chem. Soc.* **121,** 11595–11596 (1999).
21. Sun, S. *et al.* Monodisperse MFe_2O_4 (M = Fe, Co, Mn) nanoparticles. *J. Am. Chem. Soc.* **126,** 273–279 (2004).
22. Pileni, M. P. The role of soft colloidal templates in controlling the size and shape of inorganic nanocrystals. *Nature Mater.* **2,** 145–150 (2003).
23. Hyeon, T. Chemical synthesis of magnetic nanoparticles. *Chem. Comm.* 927–934 (2003).
24. Sugimoto, T. *Monodispersed Particles* (Elsevier Science, Amsterdam, 2001).
25. Kim, S. W. *et al.* Synthesis of monodisperse palladium nanoparticles. *Nano Lett.* **3,** 1289–1291 (2003).
26. Hyeon, T. *et al.* Synthesis of highly crystalline and monodisperse cobalt ferrite nanocrystals. *J. Phys. Chem. B* **106,** 6831–6833 (2002).
27. Joo, J. *et al.* Multigram scale synthesis and characterization of monodisperse tetragonal zirconia nanocrystals. *J. Am. Chem. Soc.* **125,** 6553–6557 (2003).
28. Joo, J. *et al.* Generalized and facile synthesis of semiconducting metal sulfide nanocrystals. *J. Am. Chem. Soc.* **125,** 11100–11105 (2003).
29. Peng, X. Green chemical approaches toward high-quality semiconductor nanocrystals. *Chem. Eur. J.* **8,** 334–339 (2002).

Acknowledgements

T.H. would like to thank the financial support from the Korean Ministry of Science and Technology through the National Creative Research Initiative Program. J.G.P. would like to thank the financial support by the KOSEF through the Center for Strongly Correlated Materials Research at the Seoul National University. J.H.P. would like to thank the financial support by KISTEP through X-ray/particle-beam Nanocharacterization Program.

Correspondence and requests for materials should be addressed to T. H.

Competing financial interests

The authors declare that they have no competing financial interests.